Cover Page

Universiteit Leiden

The following handle holds various files of this Leiden University dissertation:
http://hdl.handle.net/1887/59497

Author: Hooijmans, M.T.
Title: Quantitative MR in dystrophic muscle : It's more than fat
Issue Date: 2017-12-13

6

Chapter 6

Fast Multi-Station Water/Fat Imaging at 3T using DREAM-based RF Shimming

M.T. Hooijmans, O. Dzyubachyk, K. Nehrke, P. Koken, M.J.Versluis, H.E. Kan, P. Bornert

J. Magn. Reson. Imaging. 2015 Jul;42(1):217-23.

ABSTRACT

Purpose: To show the effect, efficiency and image quality improvements achievable by Dual Refocusing Echo Acquisition Mode (DREAM)-based B_1^+ shimming in whole-body MRI at 3T using the example of water/fat imaging.

Materials and methods: 3D multi-station, dual-echo mDixon Gradient Echo imaging was performed in 10 healthy subjects on a clinical 3T dual-transmit MRI system using station-to-station adapted B_1^+ shimming based on fast DREAM B_1^+ mapping. Whole-body data were obtained using conventional quadrature excitation and station-by-station adapted DREAM-based B_1^+ shimmed excitation, along with the corresponding B_1^+ maps for both excitation modes to assess image quality and RF performance.

Results: Station-dependent DREAM-based B_1^+ shimming showed significantly improved image quality in the stations covering the upper legs, pelvis and upper body region for all subjects ($p < 0.02$). This finding is supported by corresponding B_1^+ maps showing an improved B_1^+ homogeneity and a more precise nominal flip angle in the DREAM-based B_1^+ shimmed excitation ($p<0.01$). Furthermore, the very short dual-channel DREAM B_1^+ mapping times of less than 2 seconds facilitate quick B_1^+ shimming.

Conclusion: Station-dependent DREAM-based B_1^+ shimming improved RF performance and image quality and is therefore a promising technique for whole-body multi-station imaging applications.

INTRODUCTION

Whole-body magnetic resonance imaging (WB-MRI) applications are receiving more clinical attention. [1, 2]In clinical practice, many of these whole-body scans are acquired at moderate field strengths (1.5T) attributable to the sufficient image quality acquired in reasonable measuring times. [3, 4] However, due to the gain in signal-to-noise ratio (SNR) that can be traded into increased spatial resolution or scan acceleration, WB-MRI at higher field strength, like 3T, is becoming more popular. However, at these higher field strengths the effective wavelength of the RF transmit field (B_1^+) inside the patient can approach body dimensions, resulting in standing wave-kind effects, which affects the RF-field homogeneity. This can cause spatially varying image contrast and SNR, which may have serious effects on the quality of clinical diagnosis. [5]

Several approaches have been suggested to address this problem. [3, 5-7] One of the most effective emerging options is dual-channel parallel transmission that allows mitigating this problem by an enhanced control of the RF-field for each individual transmit channel. This allows B_1^+/RF shimming in a subject-specific way, adjusting the relative B_1^+ amplitudes and phases of the otherwise identical waveforms in each of the transmit channels to significantly improve B_1^+ uniformity. [5, 8, 9] However, a prerequisite for patient specific RF shimming is the knowledge about the underlying channel-specific B_1^+ maps that have to be measured with the patient in place. Most current B_1^+ mapping approaches are rather time-consuming, requiring a time-period of at least 15 s for mapping without acquiring any diagnostic data.[10-13] Therefore, especially in multi-station whole-body imaging where the RF-field can change continuously from station to station, very fast and appropriate B_1^+ mapping is required to facilitate adaptive RF shimming. Recently, a new approach for B_1^+ mapping, Dual Refocusing Echo Acquisition Mode (DREAM), which allows single shot B_1^+ mapping within a fraction of a second, was introduced. [14] Based on the quickly acquired B_1^+ maps for the individual transmit channels involved, appropriate and fast B_1^+ shimming can be performed for each individual station during multi-station imaging with the potential to meet the needs for the clinical practice. Therefore, the purpose of this study is to evaluate the effect, efficiency and image quality improvements achievable with DREAM-based B_1^+ shimming in whole-body MRI at a clinical dual-channel 3T MR system using the example of water/fat imaging.

MATERIALS AND METHODS

Study population

Ten healthy subjects (eight male/two female) participated in the study, age: 36.2±8.3 (range: 24–45 years), BMI: 24.25±3.1 kg/m^2 (range: 20.6–29.2 kg/m^2), body size: 1.81±0.09 m (range 1.65–1.92 m), and mass: 80.1±15.4 kg (range: 56–100 kg). The experiments were approved by the local institutional Ethics Committees, and all participants gave written informed consent before their enrolment in the study. Five of the participating subjects were studied at Philips Research Laboratories, Hamburg and five at Leiden University Medical Center, recruited from the LUMC radiology database.

MR technique

Whole-body multi-station data sets were acquired using clinical 3T dual-transmit MRI systems (Ingenia, Philips, Healthcare, Best, the Netherlands). The body coil was used for reception and the subjects were positioned head first in supine position. An identical MRI protocol was used in both centres, starting the data acquisition for each station with a 2D B_1^+ DREAM calibration scan, which is actually a B_1^+ mapping scan for both transmit channels (Figure 1). [14] DREAM is a magnetization prepared single shot sequence. It employs a STEAM preparation module for B_1^+ encoding and a low-angle pulse train to read-out the thus prepared magnetization, acquiring the stimulated echo (STE) and the free-induction decay (FID) signal almost simultaneously on the same readout, as gradient recalled echoes separated in time with appropriate gradient encoding. The true flip angle / B_1^+ map is derived from the ratio between the STE and FID signal, while the phase is derived from the relative transmit phase, directly adopted from one of the source images. In the present work the, the "STE first" DREAM sequence version was used The DREAM scan was centred in the middle of each station to optimize B_1^+ shimming performance. DREAM parameters: field-of-view (FoV): 450×450 mm^2, voxel size: 7×7×15 mm^3, STEAM α: 60°, imaging β: 5°, TE_{FID}/TE_{STE}/TR: 1.06/2.3/3.8 ms, shot duration: 150 ms. This dual-channel DREAM B_1^+ mapping took roughly 1.3 s per station without the use of breath holds, including a waiting time of 1 s between left and right channel transmission. The B_1^+ maps were handed over to the system's RF shim algorithm for estimation of the optimal RF amplitude gains per channel, denoted by their ratio (dB_{ratio}) and phase offsets ($\Delta\varphi$) while ensuring the SAR limits with the patient in place. Subsequently to the B_1^+ calibration scan, B_1^+ maps were obtained for the conventional quadrature transmit mode and the B_1^+ DREAM-shimmed transmit mode with similar sequence parameters as mentioned above facilitating the comparison of dual-channel shimming performance. By "quadrature" we refer to the circular

transmit mode of the unloaded coil (equal amplitudes and fixed 90° phase offset for the two RF channels). Next, two multi-station 3D dual-echo mDixon Gradient Echo acquisitions were measured with the following scan parameters: 24 contiguous axial slices, TR/TE1/TE2: 3.2/1.13/2.0 ms, FA: 5°, FoV: 520×359×120 mm³, voxel size: 1.91´1.91´5 mm³, one with DREAM-based B_1^+ shim sets and the other in quadrature mode. [15] Water/fat separation was performed as the final step after single-echo image reconstruction yielding 3D in-phase (IP), out-of-phase (OP), water, and fat images. The entire acquisition block, comprising 2D B_1^+ DREAM mapping and 3D water/fat resolved scanning (Fig. 1), is embedded in a multi-station acquisition using 16–18 stations with 10 mm station overlap. Breath-holds with duration of 19 s were solely performed for the stations covering the pelvis and chest region. The entire whole-body protocol was performed in a single run starting at the feet and had a total duration of approximately 20 minutes.

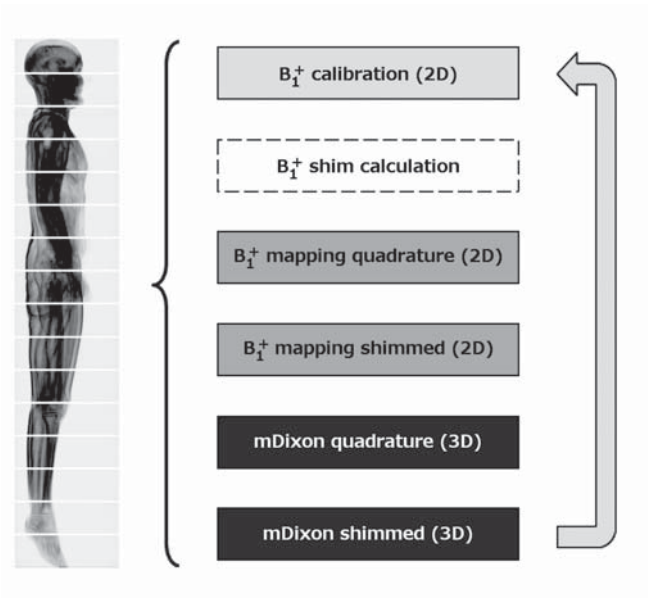

Figure 1. Illustration of the multi-station MR protocol used in this study. For each station, a set of scans was performed starting with a DREAM B_1^+ calibration scan followed by B_1^+ shim calculation. Subsequently, two DREAM B_1^+ maps were acquired to map the conventional quadrature mode RF-field and the DREAM-based B_1^+ -shimmed one, respectively. Finally, two 3D mDixon Gradient Echo scans were performed in both excitation modes. After this acquisition, the systems proceeds to the next station repeating this procedure to acquire the data for the whole multi-station protocol in one run, starting in the feet.

Image and data analysis

Image quality of the two 3D whole-body water/fat resolved scans acquired with the different excitation modes, was independently scored by three MR readers with at least 10 years' experience (MV, HK, KN) without knowledge of the B_1^+ shimming condition during image acquisition using one representative IP slice from five individual stations covering the lower leg (station 3/4), upper leg (station 6/7), pelvis (station 9/10), abdomen (station 12/13) and head (station 15/16/17) region. Scoring was performed solely on image quality using an adjusted five-point grading system [accordingly 1 (very bad) to 5 (excellent)], disregarding the part about their diagnostic value. [5] In addition to this subjective measure, a more objective image quality measure was defined using the entropy H of the normalized image intensity histogram P: $H = -\sum_{p \in P} p \log(p)$. [16] More precisely, the ratio between the histogram entropy H_{shim} for RF shimmed and H_{quad} for quadrature mode data has been used for each individual station and all image types. Values below unity indicate improved image quality on the B_1^+-shimmed volumes and vice versa. Two additional quality measures characterizing the RF field, the coefficient of variation CV, defined as the ratio between the standard deviation σ and the mean of the non-noise values in the B_1^+ map, μ: $CV = \sigma/\mu$, and the $\overline{B_1^+} = \text{mean}(B_1^+)$, were determined for each individual station for the B_1^+ maps acquired in the different excitation modes. [16] Furthermore, the DREAM-based B_1^+ shim settings, the transmit channel amplitude ratio (dB_{ratio}) and the phase offset ($\Delta\varphi$), were recorded for all stations and volunteers. To assess the overall B_1^+ shim performance, the CV, B_1^+, $\Delta\varphi$, and dB_{ratio} were averaged over all subjects and compared for each individual station. This required prior alignment of all the data sets as the subject height varied considerably, resulting in different numbers of stations required to cover the complete body of the individual volunteers. Alignment was achieved by selecting 15 stations that were represented in all the subjects. This, in particular, required disregarding the station covering the feet in all the subjects and additional removal of one station covering the upper thigh region in two of them.

Statistical analysis

The inter-observer agreement was determined with the Kendall τ_B coefficient; values higher than 0.7 were considered to indicate excellent agreement. In the case of excellent inter-observer agreement, the data was pooled for all the observers and the average scores were reported. The Wilcoxon signed-rank test has been used to determine the difference in image quality between the two excitation modes assessed with image grading. After alignment of the data sets, a paired-sample *t*-test was used to assess the difference in mean values for the CV and B_1^+ values for the different excitation modes. After grouping of the individual stations of all

subjects in five zones, classified as: the head, abdomen/chest, pelvis, upper leg and lower leg, the Kolmogorov-Smirnov test was used to test significance of the changes in CV and B_1^+ The significance level was set at $p<0.05$. All statistical analysis was performed using SPSS version 20 for Windows (SPSS Inc., Chicago).

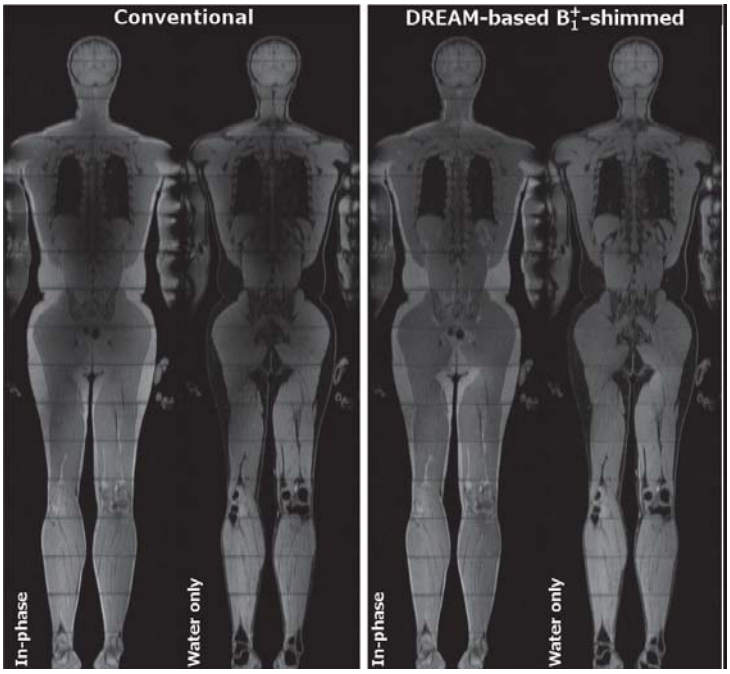

Figure 2. Coronal reformat of the entire reconstructed whole-body volumes. One coronal slice is shown from the gradient echo mDixon images of a representative subject, obtained in the conventional quadrature mode: (a) in-phase, (b) water only; and using DREAM-based B_1^+-shimmed mode: (c) in-phase and (d) water only, respectively. A significant reduction in RF shading artefacts for the DREAM-based B_1^+ shimmed case compared to the conventional quadrature situation is visible in the stations covering the torso and upper legs. The images were not further corrected for the remaining stitching artefacts; those are kept on purpose to illustrate the multi-station nature of the data.

RESULTS

All volunteer scans performed at the two different sites were successfully performed.

Image quality

The comparison of the whole-body data sets obtained with both RF excitation modes revealed a consistent improvement in image quality for all subjects in the images acquired with DREAM-based B_1^+ shimmed excitation (Figs. 2,3). The scoring of the

images showed significant improvements in the stations covering the upper leg, pelvis and upper body region (p=0.014, p<0.0001, p<0.0001), while no improvement in image quality was visible in the stations covering the lower leg and head region (p=0.28, p=0.99) (Table 1). Excellent inter-observer agreement (Kendall τ_B=0.705–0.771, p<0.01) was found between observers' grading of the images. These observer-perception-driven results were supported by the image histogram entropy ratio values of both the IP/OP and fat/water images that confirm the improvement in

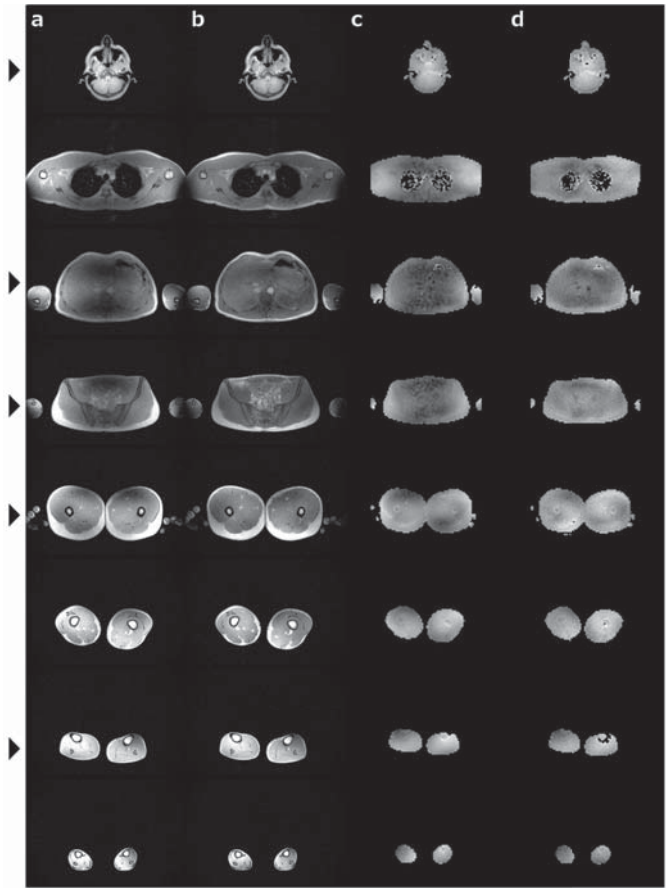

Figure 3. Axial in-phase images and corresponding B_1^+ maps for the two excitation modes. Gradient echo mDixon in-phase images of a representative subject are shown for various stations in (a) for quadrature and (b) for DREAM-based B_1^+-shimmed excitation, along with corresponding DREAM B_1^+ maps: (c) for quadrature and (d) for the B_1^+-shimmed case, respectively. Most pronounced changes consisting of less spatially varying image contrast and RF shading are visible in the upper body region. The stations marked with the arrows (left) are used for the visual grading of the image quality in this particular example; see also Table 1.

image quality (Figures 4b,c). This is especially obvious in the upper body region together with less conclusive results in the head and lower leg region compared to the human observers. In addition, a more obvious effect in image histogram entropy was visible in the water images compared to the fat images (Figures 4b,c).

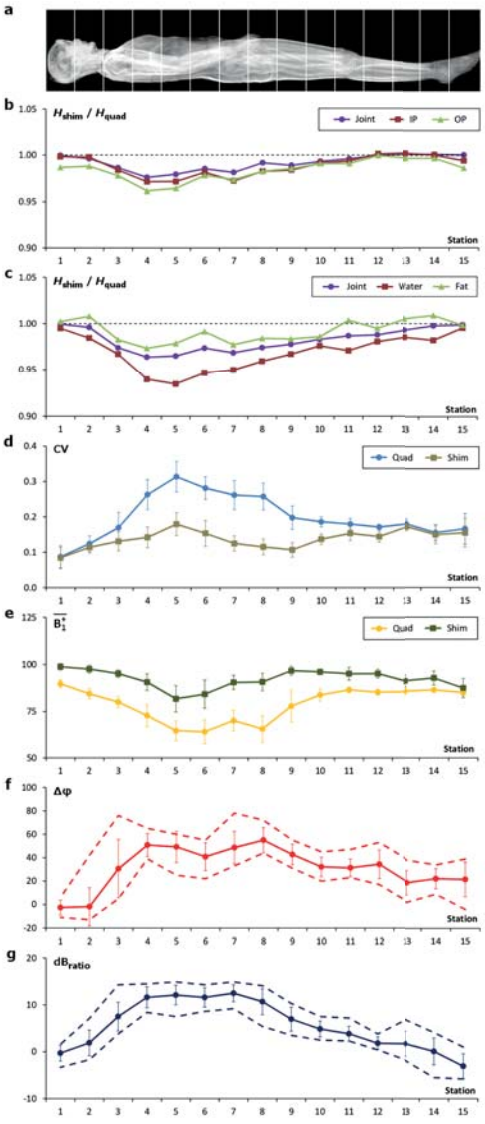

Figure 4. Summarised multi-station results averaged over the entire cohort. (a) Shows the anatomical location of each station. Data have been resampled to 15 stations, with station 1 corresponding to the head and station 15 representing the feet. The average ratio between the histogram entropy for the RF shimmed and quadrature mode excitations were calculated for IP/OP and water/fat mDixon images: (b) Shows the average histogram entropy ratios per individual station for the IP, the OP and both image types together (joint). Values below unity indicate improved image quality for the RF shimmed data. (c) Shows the histogram entropy ratios for the water-only, fat-only data and both image types together (joint), with the water-only showing significantly improved image intensity homogeneity. (d,e) Compare the measured DREAM B_1^+ maps in quadrature ("Quad") and DREAM-based shimmed ("Shim") excitation modes: (d) Shows the coefficient of variation (CV) for both excitation modes, illustrating an improvement in RF homogeneity for DREAM-based shimmed mode; a lower coefficient indicates a better homogeneity. (e) Shows the mean B_1^+, normalised to the desired/expected value (given in %) for both modes, demonstrating the better performance for the RF shimmed case. The station-dependent RF shim values (f,g) show considerable variation. In (f) the phase difference $\Delta\varphi$ (given in degree) and in (g) the amplitude ratio of the two channels (measured in dB) are shown. In subfigures (d–g), the error bars indicate standard deviation, whereas the dashed lines represent the minimum and maximum values of the corresponding variable.

	Excitation mode	Head	Abdomen / chest	Pelvis	Upper leg	Lower leg
Image quality	*Quad*	4.9±0.16	2.2±0.5	2.7±0.47	3.4±0.21	3.6±0.43
	DREAM-based RF shimmed	4.9±0.16	4.3±0.43*	4.3±0.43*	3.7±0.27*	3.7±0.44
CV	*Quad*	0.11±0.03	0.26±0.04	0.23±0.03	0.18±0.01	0.16±0.03
	DREAM-based RF shimmed	0.10±0.02	0.15±0.03*	0.12±0.02*	0.16±0.02*	0.15±0.03
B_1^+, (%)	*Quad*	87.1±2.4	70.5±5.1	74.4±6.0	85.8±1.7	85.5±1.4
	DREAM-based RF shimmed	98.1±1.9*	87.9±5.2*	93.5±3.1*	93.8±3.0*	89.9±4.4*

Table 1. Overview of the results. The mean and standard deviation for image quality according to image grading [score accordingly 1 (very bad) to 5 (excellent)], the CV, and the B_1^+ for DREAM-based RF shimmed and quadrature excitation respectively are presented for the head, abdomen, pelvis, upper leg and lower leg region. Significant differences between excitation modes are marked with an asterisk (*).

B_1^+ maps

The evaluation of the B_1^+ maps to asses overall shimming performance in both excitation modes showed an improvement in the homogeneity of the transmit RF-field using DREAM-based B_1^+ shimming, represented by a significant reduction in the CV compared to the conventional quadrature excitation: quadrature=0.20±0.03, shimmed=0.14±0.02, p<0.001 (Figs. 3,4d). This reduction is mainly found in the upper legs, pelvis and abdomen; see Table 1. In addition to the increase in B_1^+ homogeneity, a more accurate B_1^+ level was obtained with DREAM-based B_1^+ shimming: quadrature=79±4 %, shimmed=92±4 %, p<0.001; (Fig. 4e). Similar improvements were visible for all the defined zones (Table 1). Furthermore, the determined and applied B_1^+ shim sets (dB_{ratio}, $\Delta\varphi$) varied continuously throughout the stations, which is shown in Figs. 4f,g. Most pronounced changes of the shim settings were visible in the stations acquired in the shoulder-neck region, the pelvis and upper legs.

DISCUSSION

This study aimed at evaluating the effect, efficiency, and image quality improvements achievable using DREAM-based B_1^+ shimming to mitigate wave-propagation effects in whole-body imaging at 3T. Compared to conventional quadrature excitation, significant and consistent improvements in B_1^+ homogeneity and image quality are shown for multi-station water/fat imaging according to DREAM-based B_1^+ shimming per station. These improvements were obvious in stations covering the

region from the upper body to the upper legs and were consistently confirmed by three independent measures: visual subjective grading, objective evaluation of the entropy of the image histogram and reduced coefficient of variation and better nominal flip angle derived from the RF shimmed B_1^+ maps. Histogram entropy ratios were measured for the IP/OP and the water/fat volumes. For the IP/OP images, all three plots (including the joint entropy ratio estimation) clearly show improved and similar behaviour achieved due to RF shimming. However, the improvements for the water images are more obvious compared to the fat. This could be due to two reasons. First of all, fat does not show significant wave propagation effects at 3T, whereas water does. [17, 18] Having both separated can make this effect more obvious. Second, water-rich tissue is located in the body core, where wave propagation effects predominantly occur, whereas fat is often more present in the periphery and thus less affected by the field inhomogeneity.

Nevertheless, no significant improvements in image quality and RF homogeneity were found in stations covering the lower leg and head region, which suggests some station dependency in the effectiveness of RF shimming. This fact is not surprising, as the effective wavelength at 3T might not approach object dimensions in the lower legs and the head, in contradistinction to other parts of the body. However, also in those regions were no improvement in image quality and RF homogeneity was found, as well as in all the other regions in general, a more precise flip angle was measured after applying B_1^+ shimming. This indicates that the flip angle necessary to generate the correct image contrast during acquisition, is better maintained as a result of the applied B_1^+ shimming procedure per station.

It is furthermore interesting to review some of the station-dependent RF shim settings. Significant changes in the RF shim settings (dB_{ratio}, $\Delta\varphi$) with respect to quadrature mode were visible in both the shoulder/neck and leg region for all subjects. This could be explained by the asymmetrical loading of the body coil in the feed-head direction, emphasising the need for station-specific adjustments of the RF-field. Nevertheless, within consecutive stations covering the upper body region, less variation in the optimized B_1^+ shim settings was revealed, although quite substantial fluctuation between thorax and abdomen was found in some individuals. Hence, we question if region- instead of station-specific RF shimming could be sufficient for such multi-station whole-body applications. However, given that already small changes to the driving conditions of the channels can have impact on the RF performance, together with the major improvement shown in the mapping efficiency using DREAM, one could suggest that station-specific RF shimming could be recommended just as precaution.

The improvements shown with DREAM-based dual-channel RF shimming shown in this work are in line with findings of several other investigators applying RF shimming methods in the abdomen or other anatomical regions at 3T. [7, 19] However, the greatest benefit of this recently introduced DREAM B_1^+ mapping method is the time-efficiency, accelerating dual-channel B_1^+ mapping for RF shimming by an order of magnitude compared to other, rather time-consuming, B_1^+ mapping approaches. [10, 20] This allows RF transmit performance to be optimized per station during multi-station imaging applications without significant loss of scan efficiency regarding the acquisition of the desired diagnostic data. Furthermore, DREAM has the potential to be applied during very shallow or free breathing in comparison to other methods, where at least 15 seconds breath-holds are necessary to make proper adjustments to the RF-field. Apart from the gain in efficiency, this also eases system workflow, because the operator does not need to instruct the patient about potential breath-holding constraints.

One potential limitation of this study is that it solely compares DREAM-based B_1^+ shimming with the conventional quadrature excitation instead of comparing it to other RF shimming approaches. [21] However, the performance of RF shimming depending on the employed B_1^+ calibration has been recently studied by comparing DREAM to two other B_1^+ mapping approaches at a clinical dual-channel 3T MR system. [21] It was found that the RF shim results achieved with DREAM-based RF shimming were equivalent to those currently achieved with the other RF shimming methods in healthy controls. This implies that the positive effects with DREAM-based RF shimming shown in this study do not overestimate the effectiveness of this method. Secondly, only a small number of subjects participated in the study. As an improvement in image quality, flip angle accuracy and B_1^+ homogeneity due to RF shimming is not unexpected, it might has influenced some of the minor, non-significant findings in the lower leg region. The whole-body application used in this study is focussed on water/fat resolved volumetric imaging. This is of great importance in obesity-related research, where the amount and distribution of body fat are important diagnostic parameters, as well as in other systemic diseases, where the water fat distribution throughout the body is of interest. [22, 23] However, it is important to note that the effective multi-station DREAM B_1^+ mapping and shimming approach can easily be generalized to other whole-body imaging applications addressing different MR contrasts. Thereby this DREAM-based RF shimming approach could be even more beneficial in whole body imaging applications based on the more B_1^+ sensitive Spin Echo or fast Spin-Echo sequences or in imaging techniques where precise magnetization preparation is crucial as in fat suppression for example.

In conclusion, DREAM-based multi-station B_1^+ shimming showed to be very fast and effective compared to standard approaches currently available. Thereby, it achieves the desired improvements in transmit RF-field homogeneity, flip angle accuracy, image quality and workflow, suggesting that DREAM B_1^+ mapping could be of importance in clinical practice.

References

1. Nielsen YJW. Whole-body MR angiography in patients with peripheral arterial disease. Dan Med Bull 2010;57.
2. Siegel MJ, Acharyya S, Hoffer FA, et al. Whole-Body MR Imaging for Staging of Malignant Tumors in Pediatric Patients: Results of the American College of Radiology Imaging Network 6660 Trial. Radiology 2013;266:599-609.
3. Schick F. Whole-body MRI at high field: technical limits and clinical potential. Eur Radiol 2005;15:946-959.
4. Machan JS, H.; Shick, F. . Technical challenges and opportunities of whole-body magnetic resonance imaging at 3T. Physica Medica 2008: 63:70
5. Willinek WA, Gieseke J, Kukuk GM, et al. Dual-source parallel radiofrequency excitation body MR imaging compared with standard MR imaging at 3.0 T: initial clinical experience. Radiology 2010;256:966-975.
6. Kuhl CK, Traber F, Gieseke J, et al. Whole-body high-field-strength (3.0-T) MR imaging in clinical practice. Part II. Technical considerations and clinical applications. Radiology 2008;247:16-35.
7. Franklin KM, Dale BM, Merkle EM. Improvement in B1-inhomogeneity artifacts in the abdomen at 3T MR imaging using a radiofrequency cushion. J Magn Reson Imaging 2008;27:1443-1447.
8. Hoult DI, Phil D. Sensitivity and power deposition in a high-field imaging experiment. J Magn Reson Imaging 2000;12:46-67.
9. Ibrahim TS, Lee R, Abduljalil AM, Baertlein BA, Robitaille PM. Dielectric resonances and B(1) field inhomogeneity in UHFMRI: computational analysis and experimental findings. Magn Reson Imaging 2001;19:219-226.
10. Yarnykh VL. Actual flip-angle imaging in the pulsed steady state: a method for rapid three-dimensional mapping of the transmitted radiofrequency field. Magn Reson Med 2007;57:192-200.
11. Cunningham CH, Pauly JM, Nayak KS. Saturated double-angle method for rapid B1+ mapping. Magn Reson Med 2006;55:1326-1333.
12. Stollberger R, Wach P. Imaging of the active B1 field in vivo. Magn Reson Med 1996;35:246-251.
13. Sacolick LI, Wiesinger F, Hancu I, Vogel MW. B1 mapping by Bloch-Siegert shift. Magn Reson Med 2010;63:1315-1322.
14. Nehrke K, Bornert P. DREAM--a novel approach for robust, ultrafast, multislice B(1) mapping. Magn Reson Med 2012;68:1517-1526.
15. Eggers H, Brendel B, Duijndam A, Herigault G. Dual-echo Dixon imaging with flexible choice of echo times. Magn Reson Med 2011;65:96-107.
16. Belaroussi B, Milles J, Carme S, ZhuYM, Benoit-Cattin H. Intensity non-uniformity correction in MRI: existing methods and their validation. Med Image Anal 2006;10:234-246.
17. Tofts PS. Standing Waves in Uniform Water Phantoms. J Magn Reson Ser B 1994;104:143-147.
18. Dietrich O, Reiser MF, Schoenberg SO. Artifacts in 3-T MRI: physical background and reduction strategies. Eur J Radiol 2008;65:29-35.
19. Childs AS, Malik SJ, O'Regan DP, Hajnal JV. Impact of number of channels on RF shimming at 3T. MAGMA 2013;26:401-410.
20. Welch EBG, A.; berglund, J. . Quantitative whole-body fat-water MRI with R2* estimation at 3 Tesla a Custom table top for multi-station parallel imaging with a single 16-channel surface coil. Proceedings of the 20th annaul meeting of the ISMRM, Salt lake City 2013 (abstract 1524) 2013.
21. Nehrke K, Sprinkart AM, Bornert P. An in vivo comparison of the DREAM sequence with current RF shim technology. Magn Reson Mater Phy 2015;28:185-194.
22. Stranges S, Trevisan M, Dorn JM, Dmochowski J, Donahue RP. Body fat distribution, liver enzymes, and risk of hypertension: evidence from the Western New York Study. Hypertension 2005;46:1186-1193.
23. Kullberg J, Johansson L, Ahlstrom H, et al. Automated assessment of whole-body adipose tissue depots from continuously moving bed MRI: a feasibility study. J Magn Reson Imaging 2009;30:185-193.

6